Characterization of the binding properties of SIRT2 inhibitors with a *N*-(3-phenylpropenoyl)-glycine tryptamide backbone

Päivi H. Kiviranta [a,*,†], Heikki S. Salo [a,*,†], Jukka Leppänen [a], Valtteri M. Rinne [a], Sergiy Kyrylenko [b], Erkki Kuusisto [c], Tiina Suuronen [d], Antero Salminen [d,e], Antti Poso [a], Maija Lahtela-Kakkonen [a], Erik A. A. Wallén [a,‡]

[a] *Department of Pharmaceutical Chemistry, University of Kuopio, PO Box 1627, 70211 Kuopio, Finland*
[b] *Department of Biochemistry, University of Kuopio, Finland*
[c] *Department of Environmental Health, National Public Health Institute (KTL), PO Box 95, 70701 Kuopio, Finland*
[d] *Department of Neurology, Institute of Clinical Medicine, University of Kuopio, Finland*
[e] *Department of Neurology, Kuopio University Hospital, PO Box 1777, 70211 Kuopio, Finland*

ABSTRACT

SIRT2 inhibitors with a *N*-(3-phenylpropenoyl)-glycine tryptamide backbone were studied. This backbone has been developed in our group, and it is derived from a compound originally found by virtual screening. In addition, compounds with a smaller 3-phenylpropenoic acid tryptamide backbone were also included in the study. Binding modes for the new compounds and the previously reported compounds were analyzed with molecular modelling methods. The approach, which included a combination of molecular dynamics, molecular docking and cluster analysis, showed that certain docking poses were favourable despite the conformational variation in the target protein. The *N*-(3-phenylpropenoyl)-glycine tryptamide backbone is also a good backbone for SIRT2 inhibitors, and the series of compounds includes several potent SIRT2 inhibitors.

© 2008 Elsevier Ltd. All rights reserved.

1. Introduction

Human sirtuins (SIRT) consist of seven members, and they belong to the class III histone deacetylase protein family.[1,2] They are nicotinamide adenine dinucleotide (NAD^{+}) dependent enzymes, which catalyze deacetylation and mono-ADP-ribosyl transferase reactions.[1,3–5] Sirtuins are connected to several cellular processes in prokaryotic, archae and eukaryotic cells.[1,6–8] SIRT2 resides normally in the cytoplasm[1,9,10] but can move from the cytoplasm to the nucleus during mitosis, where it deacetylates Lys16 of histone H4.[11,12] It seems to be clear that SIRT2 has a role in the control of cell cycle.[13] SIRT2 has also been shown to catalyze the deacetylation of acetylated Lys40 of α-tubulin and colocalize with the cytoplasmic microtubules together with HDAC6.[13,14] The acetylation status of the microtubulin network can probably be altered by inhibition of SIRT2. It has also been shown that SIRT2 interacts with the homeobox transcription factor, HOXA10, which plays a

role in mammalian development.[15] Recent studies have provided strong evidence that the biological function of SIRT2 can be linked to glioma tumourigenesis and development of Parkinson's disease.[16,17] It has also been suggested that SIRT2 inhibitors could have favourable effects on some physiological changes involved in Parkinson's disease.[17,18]

The NAD^{+} hydrolysis product, nicotinamide, inhibits the deacetylase reaction endogenously. A3 and sirtinol were the first reported potent SIRT2 inhibitors.[19] The other known SIRT2 inhibitors are 1,4-bis[2-(4-hydroxy-phenyl)-ethylamino]-anthraquinone,[20] *para*-sirtinol,[21] EX-527,[22] *N,N′*-bis(2-hydroxybenzylidene)benzene-1,4-diamine[23] and cambinol.[24] Recently reported adenosine mimetics,[25] suramin anologues[26] and phloroglucinol derivatives[27] are also inhibitors of SIRT2. In addition, a potent and selective SIRT2 inhibitor AGK2 was recently published by Outeiro et al.[17] All reported small-molecule inhibitors inhibit SIRT2 at low micro molar level.

The first SIRT2 inhibitor with a *N*-(3-phenylpropenoyl)-glycine tryptamide backbone was compound **1**, which was found by virtual screening.[28] In an initial study the size of compound **1** was reduced, resulting in a series of *N*-(3-(4-hydroxyphenyl)-propenoyl)-amino acid tryptamides. Compounds **5** and **6** were the most potent compounds of the series (Fig. 1).[29]
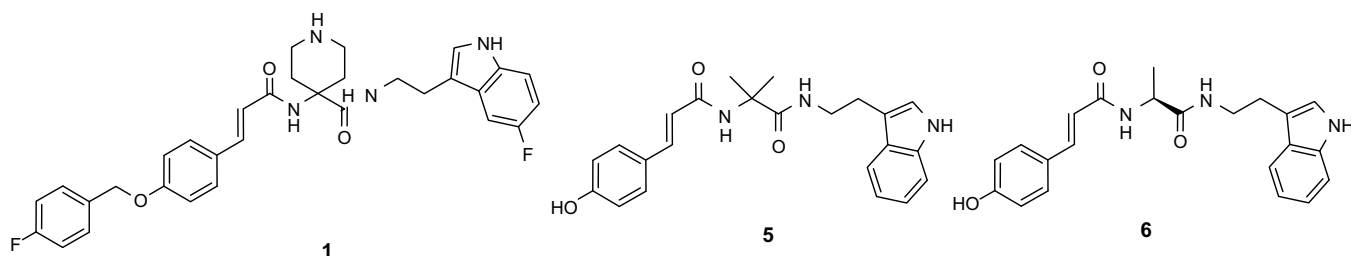
Figure 1. Compound **1** found by using virtual screening and its potent derivatives **5** and **6**.[28,29]

In order to study the *N*-(3-phenylpropenoyl)-glycine trypta-mide backbone, a new series of more modified compounds were synthesized. The modifications also included changes in the *N*-(3-phenylpropenoyl)-glycine tryptamide backbone, such as reduction of the double bond and replacing the indole ring by another aromatic ring. The new series of compounds was designed to include more variations than the earlier reported series of compounds. The study also included compounds with a shorter 3-phenylpropenoic acid tryptamide backbone.

Molecular modelling methods were used to characterize the binding and interaction properties of all compounds (also the previously reported *N*-(3-(4-hydroxyphenyl)-propenoyl)-amino acid tryptamides). So far only a little is known about the binding properties of SIRT2 inhibitors. Currently there is only one experimental crystal structure of SIRT2 publicly available.[30] As the only published structure is in apo-form it does not provide any experimental data on the binding sites and binding modes of small-molecule regulators. In order to efficiently design and screen new inhibitors more information on the interaction properties of inhibitors is urgently needed. A cavity adjacent to the active site of the protein has been hypothesized to serve as a binding site for some known sirtuin inhibitors.[17,31,32] As there is no precise information available concerning the inhibitor binding site, the area used in the search for interactions was defined to be quite large. The search was concentrated on the active site and the cavity formations around the catalytic site. The area included also the narrow, water filled, channel leading from the active site to the other site of the protein.

2. Methods

2.1. Synthetic chemistry

The new compounds **10–27** are based on a similar chemical backbone as the earlier reported compounds **1–9**, and they were synthesized by similar methods as described previously.[29] A few simplified compounds without the amino acid in the middle of the backbone were also synthesized (compounds **28–30**). General structures of the new compounds are described in Figure 2.

In amide formation reactions the carboxylic acid was activated either as an anhydride using ethyl chloroformate or pivaloyl chloride, as an acid chloride using oxalyl chloride or thionyl chloride, or as an *N*-hydroxysuccinimide ester using HOSu and DCC. The latter procedure was used for activation of the carboxylic acid terminal of L-alanine to avoid racemization.[33] More detailed synthetic procedures are described in Supplementary material.

2.2. In vitro assay for SIRT2 activity

The inhibitory activities were tested in a Fluor de Lys fluorescence-based assay. The assay was slightly modified from method described in the BioMol product sheet.

2.3. Computational procedures

The interaction possibilities between the area around the active site and the inhibitors were investigated with a molecular modelling approach, which includes a combination of molecular dynamics and molecular docking. Molecular dynamics simulations were performed in order to characterize possible conformational rearrangements in the protein structure, which could have favourable effects on ligand binding. In most docking programs the target protein is treated as a rigid structure. However, changes in the receptor structure may have drastic effects on ligand binding. Using multiple MD (molecular dynamics) snapshot conformations as target structures in the docking calculations, conformational flexibility of the protein could be incorporated in the binding mode predictions. This kind of approach has successfully been used for including receptor flexibility into docking calculations.[34,35] The target protein sets were created taking the probabilities of different protein conformations into account. The distribution of different conformational states was analyzed with cluster analysis. Based on the cluster data, cluster representatives were chosen keeping the number of cluster representatives relative to the sizes of the clusters. This way the probability distribution of the conformations in the target protein sets was similar to the distribution seen in the MD simulations.

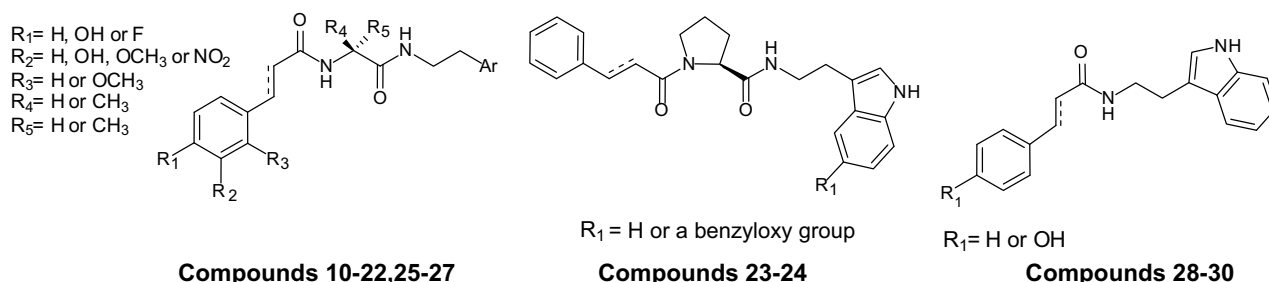R1= H, OH or F
R2= H, OH, OCH3 or NO2
R3= H or OCH3
R4= H or CH3
R5= H or CH3

Compounds 10-22,25-27

R1 = H or a benzyloxy group

Compounds 23-24

R1= H or OH

Compounds 28-30

Figure 2. The general structures of new compounds **10–30**.

3. Results and discussion

3.1. Inhibitory activities

The structures of the compounds, their inhibitory activities at 200 µM and the IC_{50} values for the most potent compounds are presented in Tables 1 and 2. The inhibitory activities are compared to the results of the earlier published compounds **1**–**9**.[29] From the presented 21 new compounds, five compounds gave an inhibition of over 50% at 200 µM (**11**, **12**, **15**, **27** and **29**), and their IC_{50} values were determined.

The earlier reported compounds showed that the central amino acids α-aminoisobutyric acid and L-alanine gave equipotent compounds, whereas the central amino acid glycine resulted in less potent compounds. All of these central amino acids were also used in the new series.

In the first group of new compounds **10**–**20** the substitution of phenyl ring was varied and the adjacent double bond was reduced. Compounds **11**, **12** and **15** gave over 50% inhibition at 200 µM. Compounds **11** and **12** without the substituent on the phenyl ring gave inhibitions of 49.5% and 59.6% at 200 µM and IC_{50} values of 100 µM and 109 µM, respectively. Compound **15** with the *para*-fluoro substituent on the phenyl ring gave an inhibition of 61.3% at 200 µM and an IC_{50} of 105 µM. These compounds are not as potent as the corresponding earlier reported *para*-hydroxy substituted compounds **5** and **6**, but more potent than the corresponding *meta*-hydroxy and *meta*- or *ortho*-methoxy substituted compounds **10**, **13** and **14**. Also a *meta*-nitro substituted compound **16** gave an equipotent inhibitory activity with compound **13**.

Replacing the central amino acid alanine by glycine gave **17** and **18**, which gave the lower inhibitory activities, 22.7% and 24.2% at 200 µM, respectively. Reduction of the adjacent double bond of the phenyl group resulted in compounds **19** and **20**. Increased flexibility decreased the inhibitory activity. These two compounds were clearly less potent than the corresponding compounds **11** and **5** with the double bond, respectively.

The second group of compounds constitute **21** and **22** where the indole ring has been replaced by a 3-pyridyl and a phenyl ring. These compounds gave lower inhibitory activities as compared to the corresponding indole ring containing compounds **5** and **12**. The 3-pyridyl ring reduced the inhibitory activity strongly, whereas the phenyl ring only lowered the inhibitory activity slightly.

The effect of a more rigid central amino acid proline was studied with compounds **23** and **24**. Compound **23** has an intermediate inhibitory activity as compared to compounds **12** and **17** with the central amino acids L-alanine and glycine, respectively. The third group of compounds constitute **24**–**27**, which have a benzyloxy group in 5-position of the indole ring. The benzyloxy group did not have a significant effect on the inhibitory activity. Also a similar effect was observed with a methoxy group in the 5-position of the indole ring in compound **18**. However, compound **27** with a reduced double bond in combination with a benzyloxy group in the 5-position of the indole ring gave a good inhibitory activity, with an inhibition of 50.2% at 200 µM and an IC_{50} value of 86 µM. It was even slightly more potent than the corresponding compound with a double bond **25** and the other reduced compounds without the benzyloxy substituents **19** and **20**.

The fourth group of compounds **28**–**30** with the shorter 3-phenylpropenoic acid tryptamide backbone are presented in Table 2. Interestingly, this group of relatively small compounds gave good inhibitory activities as compared to compounds discussed above. The best compound **29** gave an inhibition of 58.0% at 200 µM and an IC_{50} of 173 µM.

3.2. Binding mode prediction

The binding possibilities of the reported compounds were investigated by analyzing the docking poses of the most potent compound belonging to the series, compound **6**, and then comparing the docking poses of the other compounds with these results. The docking poses obtained from the docking calculations were analyzed with cluster analysis in order to distinguish docking poses, which occur frequently in the docking calculations (Fig. 3). The clustering of the binding modes was performed based on root mean square deviation (RMSD) values calculated on heavy atoms of the ligands. Based on the cluster data the possible interactions and calculated scoring values of different binding modes were analyzed.

The docking results obtained using the protein conformations from the three individual molecular dynamics runs, MD run 1, MD run 2 and MD run 3 (referred later as **MD1**, **MD2**, **MD3a** and **MD3b**, see details in Section 5), were analyzed separately. The docking poses seen in these dockings were compared to the poses obtained for compound **6** in the docking runs performed using the X-ray crystal conformation of the protein as a target structure. Of the 15 docking runs performed on each ligand MD snapshot pair, three best-ranked solutions were chosen for the set of conformations, which was subjected to cluster analysis with a hierarchical average-linkage cluster method. The cluster analysis was done in order to see which docking poses were ranked high when sets of distinct target protein structures were used in the dockings.

Visual inspection of the cluster data of the docking results of compound **6** revealed that the docking poses clearly were divided into distinct binding modes. In order to determine the frequency of different binding modes a cut-off value for the cluster formation had to be defined. Choosing the right cut-off level is crucial step in the analysis of the data obtained with hierarchical cluster methods[36] as it determines the sizes and the homogeneities of the formed clusters.[36] The cut-off level of the clustering was first determined by applying the Kelley–Gardner–Sutcliffe (KGS) function.[37] However, visual inspection of the cluster members showed that KGS led in this case to too high cut-off levels. Members belonging to the same cluster were observed to have substructures located in distinct adjacent binding pockets on the protein surface. Thus, the cut-off level was reduced based on visual inspection of the cluster members, and a cut-off value of 3.2 Å was used in the analysis.

The distribution of the cluster sizes showed that certain binding modes occurred clearly more frequently than others. Interestingly, the most common docking pose for **6** was similar in all of the four individual dockings performed on the MD snapshots and, also, in the dockings performed on the crystal structure. Despite the differences in the MD simulation length, protonation of His187 and the used scoring function of the different docking runs, a similar binding mode was found to be the most common docking solution for the compound.

The binding mode (referred later as binding mode **A**), which was seen as the most frequent docking pose in all of the individual docking series, had the *para*-hydroxyphenyl group of the ligand located in a narrow channel leading from the active site to the opposite site of the protein. The phenyl ring is surrounded by the residues Ile93, Pro94, Leu138 and Leu103. The indole ring is situated in a hydrophobic cavity formed between residues His187 and Phe119, which is the area where the acetylated lysine of the substrate is shown to bind.[38] Due to variation in the side-chain conformations in this protein area (especially His187), the biggest clusters included also poses, which had the indole ring oriented slightly towards the cavity close to Phe96, Phe119, and Tyr104.

The binding mode **A** offers several hydrogen bonding possibilities for **6**. The backbone carbonyl group of Glu137 could serve as a

Table 1
SIRT2 inhibitors with *N*-(3-phenylpropenoyl)-glycine tryptamide backbone (95% confidence intervals for IC$_{50}$ given in parentheses)
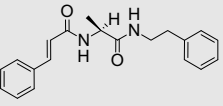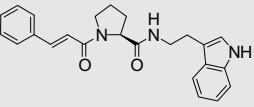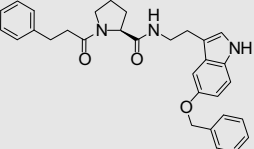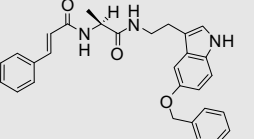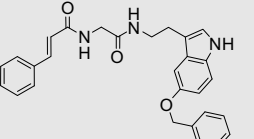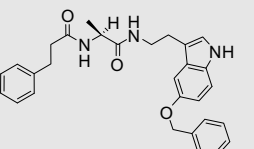
Compound	Structure	Inhibition 200 μM ± SD,[a] % SIRT2	IC$_{50}$ (μM) SIRT2[b]
1[29]		77.3 ± 4.8	51 (27–75)
2[29]		79.1 ± 1.4	63 (41–96)
3[29]		32.6 ± 18.2	–
4[29]		55.4 ± 3.3	99 (66–150)
5[29]		83.3 ± 3.7	50 (23–109)
6[29]		88.6 ± 0.8	47 (28–79)
7[29]		8.5 ± 6.0	–
8[29]		44.3 ± 10.6	–
9[29]		67.5 ± 1.1	80 (53–120)
10		46.7 ± 0.1	–

Table 1 (*continued*)
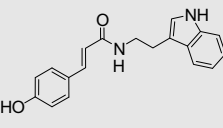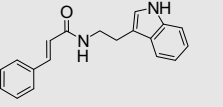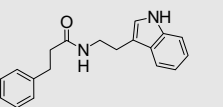
Compound	Structure	Inhibition 200 μM ± SD,[a] % SIRT2	IC$_{50}$ (μM) SIRT2[b]
11		49.5 ± 0.7	100 (71–141)
12		59.6 ± 11.3	109 (49–243)
13		45.9 ± 15.5	–
14		35.0 ± 8.5	–
15		61.3 ± 0.5	105 (53–209)
16		42.1 ± 15.3	–
17		22.7 ± 11.9	–
18		24.2 ± 3.7	–
19		12.5 ± 1.3	–
20		19.5 ± 1.2	–
21		2.0 ± 2.8	–

Table 1 (continued)

Compound	Structure	Inhibition 200 μM ± SD,[a] % SIRT2	IC$_{50}$ (μM) SIRT2[b]
22		29.6 ± 1.8	–
23		36.6 ± 8.4	–
24		29.8 ± 3.2	–
25		43.7 ± 2.7	–
26		32.9 ± 2.3	–
27		50.2 ± 1.1	86 (34–216)

[a] SD, standard deviation.
[b] IC$_{50}$ were determined for compounds which had over 50% inhibition at 200 μM for SIRT2.

Table 2
SIRT2 inhibitors with 3-phenylpropenoic acid tryptamide backbone (95% confidence intervals for IC$_{50}$ given in parentheses)

Compound	Structure	Inhibition 200 μM ± SD,[a] % SIRT2	IC$_{50}$ (μM) SIRT2[b]
28		44.3 ± 4.1	–
29		58.0 ± 11.1	173 (108–276)
30		44.1 ± 7.4	–

[a] SD, standard deviation.
[b] IC$_{50}$ were determined for compounds which had over 50% inhibition at 200 μM for SIRT2.

hydrogen bond acceptor for the hydroxyl group attached to the phenyl ring. There are several other hydrogen bond possibilities for a hydroxyl group deeper in the channel. The cut-off value in the clustering allowed some variation in the position of the *para*-hydroxyphenyl among the members of the biggest cluster. Deeper in the pocket backbone amines of Gly141, Gln142 and Phe143 could act as hydrogen bond donors and the backbone carbonyl group of Tyr139 as an acceptor for a hydroxyl group. The binding mode **A** allows the amide bond of the compound, located closer to the *para*-hydroxyphenyl group, to form a hydrogen bond either with the backbone amine of Ile169 or with the carboxylate group of Asp170. Both orientations for the amide bond were seen among the solutions of these clusters.

The docking solutions of binding mode **A** had obtained fairly high scoring values by the scoring functions. In the dockings performed on the crystal structure and in the docking series of **MD3b** the largest cluster included the best-ranked solution. The clusters of the binding mode **A** in **MD1**, **MD2** and **MD3a** were all ranked among the best clusters when the ranking was made based on the best-scored individual found in the cluster.

The best-ranked docking poses on each MD docking series of **6** had the *para*-hydroxyphenyl structure placed in the channel leading through the protein. In the best-ranked solution of **MD1** and **MD2** the indole ring is located in a pocket formed by residues Ala85, Ser88, Gly92, Ile93, Pro94, Asp95, Phe96 and Arg97. The best-ranked docking conformations in **MD1** and **MD2** were very close to each other. In **MD3a** the *para*-hydroxyphenyl group is placed slightly different than in **MD1** and **MD2**. The indole ring is under the flexible loop, but has a slightly different orientation as in **MD2**, allowing the indole nitrogen to form a hydrogen bond with Asp170. In **MD1** and **MD2** the amide nitrogens are able to form a hydrogen bond to the side chain of Asp170. Also a hydrogen bond between the other amide nitrogen and the backbone carbonyl of Ile169 could be possible. In **MD3a** similar hydrogen bond formation between the amide structures and the residues cannot be seen. This probably causes some difference in the location of the indole ring. The binding mode seen in the highest-scored solutions in **MD1**, **MD2**, and **MD3a** is later referred as binding mode **B**. As stated earlier the highest-scored docking pose of **MD3b** was the most often occurring binding mode **A**. The highest-scored conformation placed the *para*-hydroxyphenyl group in a position allowing the hydroxyl group to form hydrogen bonds with the side-chain carbonyl group of Gln142, and the indole-side amide bond carbonyl formed a hydrogen bond with Ile169.

Although the biggest clusters in all MD runs were similar there were some variations in the sizes and binding modes of the other clusters. In the docking performed using the protein conformations of **MD1** run two distinct binding modes clearly occurred more frequently than the others. The two most populated clusters were almost similar in size. The docking poses in the second biggest cluster differ significantly from the conformations in the binding modes **A** and **B**. In these docking poses the *para*-hydroxyphenyl ring is located in the hydrophobic cavity between His187 and Phe119. The indole ring is located in a pocket formed by residues Ala85, Ser88, Gly92, Ile93, Pro94, Asp95, Phe96 and Arg97. The fact that this binding mode is the only frequently occurring binding mode, which does not involve entering the narrow channel, makes this binding mode interesting. This binding mode is later referred as binding mode **C**. The binding mode of the third most populated cluster in **MD1** was binding mode **B** as the *para*-hydroxyphenyl structure is buried in the narrow channel and the indole ring is located in the pocket near residues Ala85, Ser88, Gly92, Ile93, Pro94, Asp95, Phe96 and Arg97.

As the first two clusters in **MD1** were practically equally sized, in **MD2** the most populated cluster is significantly larger in size than the other clusters. In **MD2** 86% of the docking poses had the
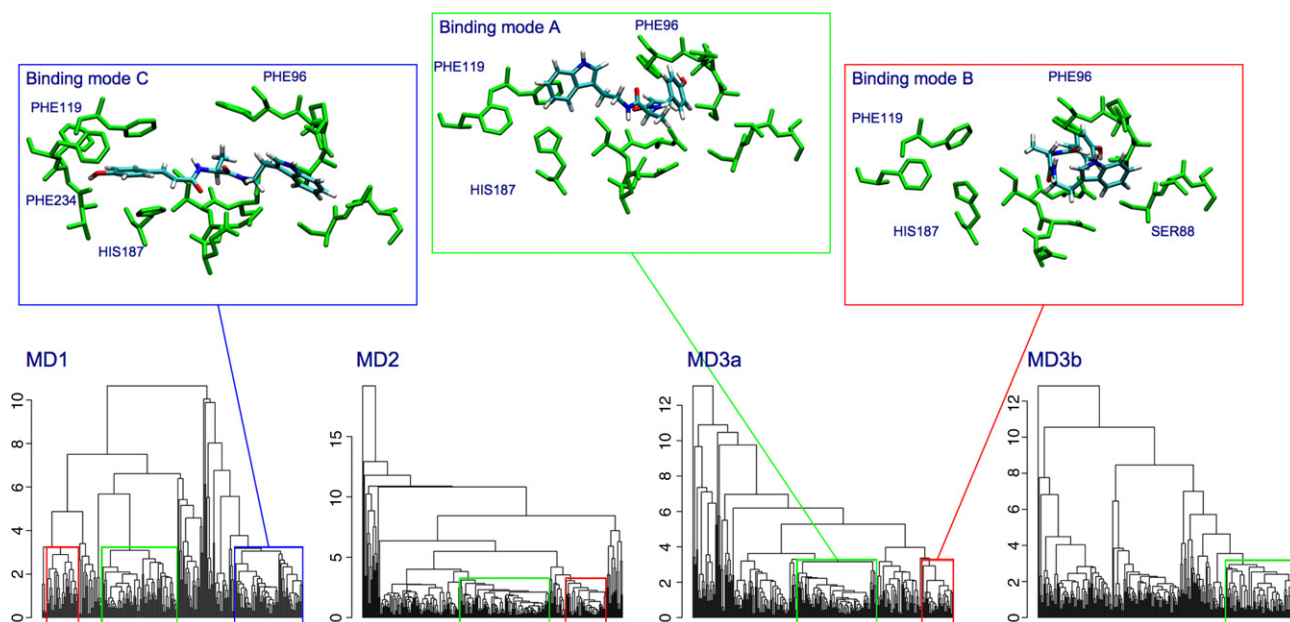
Figure 3. Dendrograms representing the cluster data of compound **6** in docking series **MD1**, **MD2**, **MD3a** and **MD3b**. The green rectangle illustrates the clusters of binding mode **A**, the red binding mode **B** and the blue binding mode **C**.

para-hydroxyphenyl group located in the narrow channel. In the case of **MD1** only 52% of the docking poses had the *para*-hydroxyphenyl group in this area. In the **MD2** dockings binding poses similar to the ones in cluster 2 of **MD1** were extremely rare. This could be explained by frequency of the different conformational forms of the active site residues in the used target protein set. The simulation length of **MD1** was significantly shorter than in **MD2** and **MD3**. Because of this the distribution of conformational states could differ from that of the longer simulations. In **MD2**, **MD3a** and **MD3b** the target protein sets were created based on cluster analysis and, in these sets, the significance of the frequent conformational states is therefore emphasized. This might, respectively, reduce the significance of the protein conformations, which would favour docking poses similar to the cluster 2 in **MD1**, if these conformations do not occur frequently in the simulation. One apparent difference between the conformations of target proteins of **MD1** and **MD2** could be seen in the conformational states of the side chain of His187. In the shorter molecular dynamics run of **MD1** the conformation of His187 remains close to the conformation seen in the crystal structure. However, in the long 10 ns, **MD2** run, the conformation of His187 changes dramatically before 1 ns and the conformation remains similar throughout the rest of the simulation.

In the **MD3a** most frequent docking pose was similar to the most common binding mode in the **MD2** docking calculations. In the protein structures of **MD3** the distribution of the conformational states of His187 varies from the one of **MD2**. His187 could be found more often in the conformation close to the conformation seen in the crystal structure than in the structures of **MD2**. Also in the case of **MD3a** over 80% of the docking poses belonged to clusters, which had the *para*-hydroxyphenyl group in the channel. Docking poses similar to binding mode **C** were only rarely observed.

Based on the cluster analysis of the docking results of **MD1**, **MD2**, **MD3a** and **MD3b** the most frequently occurring binding modes were chosen for further analysis (binding mode **A**). The binding mode, which had obtained the highest score in **MD1**, **MD2** and **MD3a**, was also chosen for further characterization (binding mode **B**). In both of these binding modes the *para*-hydroxyphenyl group was located in the channel, and only the po-

sition of the indole ring varied. In order to include a frequently occurring binding mode, which does not bind into the channel, into further analysis the second biggest cluster of **MD1** was chosen (binding mode **C**). Although the **MD1** differs from the **MD2**, **MD3a** and **MD3b** in the length of the simulation and in the approach used in the protein conformation selection, as one of the frequent binding modes in these calculations was significantly different than the frequent docking poses in other MDs, it was necessary to include this binding mode for further analysis.

3.3. SAR

The effect of structural modifications of the reported compounds on the binding properties was analyzed by investigating the docking poses resembling the binding modes **A**, **B** and **C** of compound **6**. The ability of the used scoring functions to rank the compounds according to the biological activity data was also tested.

Accurate prediction of the binding affinity seems to be an extremely difficult task for the scoring functions of the available docking programs. This problem has been a widely acknowledged weakpoint in the most currently available docking applications.[39,40] As anticipated, the scoring function was not able to create a correct rank-ordering for the compounds. When the ranking and scoring was based on the scoring value of the highest-scored solution on each MD run, no correlation could be seen between the scoring values and the inhibition percentages. There was no difference between the performance of the two distinct scoring functions, Goldscore and Chemscore used in **MD3a** and **MD3b**. Neither was there difference between **MD1**, **MD2**, **MD3a** and **MD3b**. In order to test the effect of the structural variation in the used target structures mean fitness scores were calculated for each compound using the three best-ranked docking solution on each ligand–protein pair. The rationale behind this idea is in the fact that as the target protein structures are chosen based on the occurrence frequency in the MD simulation, compounds, which get higher scores on common target conformations, would get higher mean scores. However, in this case this approach neither gave any correlation between the calculated scores and the biological data. The fact that

the activity range of the compounds in this study is quite small, the correct rank-scoring and activity prediction would require high accuracy from the scoring function.

The results of cluster analysis of the docking poses of the other docked compounds were in general terms similar to the results of compound **6**. In the **MD1** the most common binding pose for almost all of the compounds is the binding mode in which the phenyl ring is located in the hydrophobic cavity between Phe119 and His187, and the indole part of the compound is located under the loop structure of Pro94, Asp95 and Phe96 (binding mode **C**). In the dockings of **MD2** the most frequently occurring binding pose for most compounds resembled the binding mode **A** of **6**. Some variation could be seen in the orientation of the indole ring as the indole ring could be seen oriented slightly towards the cavity close to Phe96, Phe119 and Tyr104. The most frequent binding mode for some compounds, for example, compounds **8**, **28**, **29** and **30**, had the *para*-hydroxyphenyl in the channel, but the indole ring is located under the loop structure formed by residues Ala85, Ser88, Gly92, Ile93, Pro94, Asp95, Phe96 and Arg97 resembling the binding mode **B**. Also in **MD3a** the highest-populated clusters of most compounds were similar to the binding mode **A**. The biggest clusters of compounds **8**, **28**, **29** and **30** had a binding conformation similar to the binding mode **B**. In **MD3b** the highest-populated clusters included a wider range of different binding modes.

The differently substituted phenyl groups showed that a hydroxyl group in the *para*-position of the phenyl ring had a positive effect on the inhibitory activity. Compounds **5**, **6** and **9** had an inhibition in the range 67.5–88.6% at 200 μM. In binding modes **A** and **B** hydrogen bonding possibilities for a hydroxyl group can be found at the end of the narrow channel. Compounds without a hydroxyl group in this position cannot form these interactions. In these binding modes any of the substituents, which compounds **10**, **13**, **14** and **16** have in the *meta*- and *ortho*-positions, do not offer any hydrogen bond interaction possibilities. Neither does the binding mode offer the hydrogen bond possibility for compound **4** that has a methoxy substituent in *para*-position. However, compound **4** gave an inhibition of 55.4% at 200 μM and IC$_{50}$ was 99 μM.[29] Binding mode **C** also offers a hydrogen bond possibility for a hydroxyl group in the *para*-position. The same as in the binding modes **A** and **B**, the binding mode **C** does not offer additional hydrogen bonding interactions for structures with other substituents or substituents in other positions.

Changes made to the central amino acids located between the amide structures had various effects on the inhibitory activity. Changing the alanine residue of **6** to glycine residue of **8** or proline residue of **23** lowered the inhibition to 40% at 200 μM. However, changing the alanine residue of **6** or **12** to α-aminoisobutyric acid in **5** or **11** had no effect on the inhibitory activity. Explanations for the effect of such small changes could not be easily found based on the binding modes. The proline residue could restrict forming low energy conformations, which would allow favourable interactions with the protein. In the case of the glycine residue the inhibitory activity could be affected by the increased conformational flexibility. As the flexibility increases the binding process has larger negative effect on the entropic term of the binding free energy as in the case of more rigid compounds.

Compounds **11** and **12** gave higher inhibitions of 49.5% and 59.6% at 200 μM than similar compounds **21** and **22** with the indole ring replaced by other aryl groups. The inhibitory activities of **21** and **22** were 2.0% and 29.6% at 200 μM, respectively. This clearly indicates that the indole ring is forming important interactions in the binding site. The interactions of the indole ring in all of the binding modes **A**, **B** and **C** are mainly hydrophobic and aromatic interactions. Similar interactions are also possible for compounds **21** and **22**. The larger molecular structure of the indole

ring could, however, make such interactions stronger. Compound **21** had obtained low scoring values in both scoring functions and in all individual docking series. A clear difference could not be seen in the binding modes of these compounds.

Addition of a benzyloxy group to the 5-position of the indole ring of compounds **12** and **17** resulting in compounds **25** and **26** had no effect on the inhibitory activity. Compounds **12** and **25** had inhibitions in the range of 59.6–43.7% at 200 μM, and compounds **17** and **26** had inhibitions in the range 22.7–32.9% at 200 μM. As increased molecular structure offers more interactions upon binding and thus higher inhibitory activity, the fact that the inhibitory activity does not increase indicate that there are no favourable interaction partners for the benzyloxy group in the binding site. However, both of the used scoring functions clearly overestimated the binding affinity of these structures. The larger molecular structure led to higher scoring values in all of the individual docking series, **MD1**, **MD2**, **MD3a** and **MD3b**. The results of the cluster analysis also indicate that single favourable interaction site for the benzyloxy group was not found in the docking runs. A wider variety of docking poses were created in the docking process for these larger compounds, which could be seen as smaller cluster sizes.

In addition, the relatively small compounds **28**–**30** were almost equipotent. The inhibitory activities of **28**, **29** and **30** were 44.3%, 58.0% and 44.1% at 200 μM, respectively, and the IC$_{50}$ value of **29** was 173 μM. In **MD2** and **MD3a** the most frequent binding mode for these compounds had the *para*-hydroxyphenyl group placed in the narrow channel, and the docking poses were similar to binding mode **B**. In **MD1** the compounds **29** and **30** had often docking poses resembling binding mode **C** as for **28** the binding mode **B** occurred most frequently. In **MD3b** a wider variety of different docking poses were observed. The *para*-hydroxy substituent on phenyl ring did not seem to be as important for the inhibitory activity among these compounds as in the case of the bigger compounds. Removal of the *para*-hydroxy substituent of **28** did not lower the inhibitory activity. Neither did the removal of the double bond in the propenoyl side-chain lower the inhibitory activity. These differences could raise the question whether the binding of these smaller compounds differs from the binding of the other compounds. However, these modelling results do not explain this, and further studies would be needed.

Compound **28** is also a known natural product isolated from kernels of maize, safflower seed and *Ravensara anisata* Danguy, among others.[41–43]

4. Conclusion

The most potent new compounds were **11**, **12**, **15**, **27** and **29** with IC$_{50}$ values in the range 86–173 μM. As compared to the best earlier reported compounds with the same backbone **5** and **6** with IC$_{50}$ values in the range 47–50 μM, these new compounds did not lead to an improvement of the inhibitory activity. However, the new compounds clearly indicate that the *N*-(3-phenylpropenoyl)-glycine tryptamide backbone is a good backbone for the design of SIRT2 inhibitors. One-third of the synthesized compounds have over 50% inhibition at the concentration of 200 μM. In addition, the study revealed that a series of compounds with a smaller 3-phenylpropenoic acid tryptamide backbone also were good SIRT2 inhibitors.

Molecular modelling methods were used for analyzing possible binding modes for all the compounds. Molecular docking calculations were performed using several sets of protein conformations obtained from molecular dynamics simulations. The used sets of protein conformations were created using cluster analysis and choosing cluster representatives based on the relative sizes of the

clusters. Cluster analysis was also used for the investigation of the binding poses obtained in the docking runs. Based on the cluster data of the docking poses three distinct binding modes clearly stand out from the results. The binding mode **A** was found to be a common binding mode in all of the MD dockings and with most of the compounds. The binding mode occurred frequently despite the difference in the His187 protonation state and the used scoring function. The binding mode **B** stands out as this binding mode seemed to obtain high scoring values in **MD1**, **MD2** and **MD3a**. The third binding mode, which clearly stands out from the results, is the binding mode **C**. This binding mode was frequent in **MD1** for most of the compounds but was only rarely seen in **MD2**, **MD3a** and **MD3b**.

The study gave important information about how the compounds interact with SIRT2. Reasonable binding modes were found for these compounds in the area, which has been earlier postulated as a binding site for sirtuin inhibitors. However, prediction of a binding mode without experimental structural data is an extremely challenging task. In this study binding modes, which had obtained high scoring values despite the variation in the target structure, were studied. In future we are planning to perform extensive free energy calculations for evaluating the binding affinity of the compounds in the binding modes, which were observed in this study. These free energy calculations may provide further validation for the binding mode predictions.

5. Experimental

5.1. In vitro assay for SIRT2 activity

The Fluor de Lys fluorescence assays were modified from method described in the BioMol product sheet. Briefly, assay was carried out using Fluor de Lys-acetylated 250 μM SIRT2-peptide substrate (KI-179), 500 μM NAD⁺ (N6522, Sigma), recombinant GST-SIRT2-enzyme and SIRT2-assay buffer (HDAC assay buffer, KI-143, supplemented with 1 mg/mL BSA, A3803, Sigma). GST-SIRT2-enzyme was produced as described recently.[20] The buffer, SIRT2-enzyme, NAD⁺ and DMSO/compounds in DMSO (2.5 μL in 50 μL total volume of reaction mixture; DMSO from Sigma, D2650) for testing were preincubated for 5 min at room temperature. The reaction was started by adding the substrate, and the reaction mixture was incubated for 3 h at 37 °C. After that Fluor de Lys-developer (KI-176) plus 2 mM nicotinamide in 50 μL were added, and incubation was continued for 45 min at 37 °C. Fluorescence readings were obtained using the Victor™ 1420 Multilabel Counter (Wallac, Finland) with excitation wavelength 360 nm and emission 460 nm. Each experiment was repeated at least three times.

5.2. Computational details

5.2.1. Molecular dynamics

The molecular dynamics runs were performed using the GROMACS 3.3.1 software package[44] with GROMOS96[45] force field. The monomer B of the crystal structure of SIRT2 (pdb code: 1J8F) was used as the starting geometry for the simulations. SPC water model,[46] PME electrostatics,[47,48] Berendsen pressure and temperature coupling[49] and periodic boundary conditions were applied in the simulations. After initial minimizations and equilibration runs three distinct MD runs were performed. A 400 ps and two separate 10 ns MD runs were performed holding the backbone atoms fixed. The two 10 ns fixed backbone simulations differed in the protonation state of His187. A set of protein conformations was chosen from the fixed-backbone MD simulations to be used as target structures in molecular docking calculations. Eighty-one protein conformations were obtained from the 400 ps MD run by taking

snapshots from the trajectory at a regular 5 ps time interval (**MD1**). The protein conformations from the 10 ns side-chain MD runs (**MD2** and **MD3**) were obtained based on a RMSD cluster analysis of the active site side-chain conformations. The clusterings were performed with the g_cluster program implemented in GROMACS using the gromos cluster method.[50] The clustering included 10,000 snapshots from the 10 ns MD trajectory, and was made using RMSD value of 1.0 Å as a cut-off distance defining the cluster size. The pool of conformations was reduced to 95 conformations in **MD2** and 92 in **MD3** keeping the proportions of cluster representatives and the size of the original clusters constant. All of the conformations were minimized in GROMACS with steepest descent. Prior to using the conformations as docking targets all hydrogens were added to the protein structures with the BIOPOLYMER module of Sybyl 7.3.3.[51]

5.2.2. Molecular docking

The 3D ligand structures of the inhibitors used in the docking were built with the sketch module of Sybyl 7.3.3. The compounds were minimized with Powell minimization method using a convergence criterion of 0.05 kcal/molÅ until the convergence was reached. MMFF94 charges were assigned to the atoms of the ligand compounds. The docking calculations were performed with version 3.2 of Gold docking software.[52] The search area for the docking program was defined by choosing residues within 15 Å from Ile169 to represent the active site of the protein and by applying the cavity detection method of Gold. For each ligand 15 docking runs were performed, and the docking poses were scored with Goldscore scoring function in **MD1**, **MD2** and **MD3a** and with Chemscore scoring function in **MD3b**. Three binding poses for each ligand–protein pair were chosen for further analysis based on the obtained scoring values. The binding poses were clustered within each ligand, and frequently occurring docking modes were detected. The selected binding modes were clustered with a hierarchical average-linkage clustering method based on atom pair RMSD values.[53] The cluster height for the hierarchical clustering was chosen based on KGS function[37] and visual inspection of the formed clusters.

Supplementary data

Detailed experimental procedures for the syntheses, NMR spectra, ESI-MS results and elemental analysis data for the new compounds, and in vitro assay for SIRT2 activity are available. Supplementary material associated with this article can be found in the online version. Supplementary data associated with this article can be found, in the online version, at doi:10.1016/j.bmc.2008.07.059.

References and notes

1. Sauve, A. A.; Wolberger, C.; Schramm, V. L.; Boeke, J. D. *Annu. Rev. Biochem.* **2006**, *75*, 435.

2. Smith, J. S.; Brachmann, C. B.; Celic, I.; Kenna, M. A.; Muhammad, S.; Starai, V. J.; Avalos, J. L.; Escalante-Semerena, J. C.; Grubmeyer, C.; Wolberger, C.; Boeke, J. D. *Proc. Natl. Acad. Sci. U.S.A.* **2000**, *97*, 6658.
3. Tanner, K. G.; Landry, J.; Sternglanz, R.; Denu, J. M. *Proc. Natl. Acad. Sci. U.S.A.* **2000**, *97*, 14178.
4. Smith, B. C.; Denu, J. M. *Biochemistry* **2006**, *45*, 272.
5. Michan, S.; Sinclair, D. *Biochem. J.* **2007**, *404*, 1.
6. Brachmann, C. B.; Sherman, J. M.; Devine, S. E.; Cameron, E. E.; Pillus, L.; Boeke, J. D. *Genes Dev.* **1995**, *9*, 2888.
7. Guarente, L. *Genes Dev.* **2000**, *14*, 1021.
8. Lin, S. J.; Ford, E.; Haigis, M.; Liszt, G.; Guarente, L. *Genes Dev.* **2004**, *18*, 12.
9. Frye, R. A. *Biochem. Biophys. Res. Commun.* **2000**, *273*, 793.
10. Afshar, G.; Murnane, J. P. *Gene* **1999**, *234*, 161.
11. Vaquero, A.; Scher, M. B.; Lee, D. H.; Sutton, A.; Cheng, H. L.; Alt, F. W.; Serrano, L.; Sternglanz, R.; Reinberg, D. *Genes Dev.* **2006**.
12. Inoue, T.; Hiratsuka, M.; Osaki, M.; Yamada, H.; Kishimoto, I.; Yamaguchi, S.; Nakano, S.; Katoh, M.; Ito, H.; Oshimura, M. *Oncogene* **2007**, *26*, 945.
13. North, B. J.; Marshall, B. L.; Borra, M. T.; Denu, J. M.; Verdin, E. *Mol. Cell* **2003**, *11*, 437.
14. Hubbert, C.; Guardiola, A.; Shao, R.; Kawaguchi, Y.; Ito, A.; Nixon, A.; Yoshida, M.; Wang, X. F.; Yao, T. P. *Nature* **2002**, *417*, 455.
15. Bae, N. S.; Swanson, M. J.; Vassilev, A.; Howard, B. H. *J. Biochem. (Tokyo)* **2004**, *135*, 695.
16. Hiratsuka, M.; Inoue, T.; Toda, T.; Kimura, N.; Shirayoshi, Y.; Kamitani, H.; Watanabe, T.; Ohama, E.; Tahimic, C. G.; Kurimasa, A.; Oshimura, M. *Biochem. Biophys. Res. Commun.* **2003**, *309*, 558.
17. Outeiro, T. F.; Kontopoulos, E.; Altmann, S. M.; Kufareva, I.; Strathearn, K. E.; Amore, A. M.; Volk, C. B.; Maxwell, M. M.; Rochet, J. C.; McLean, P. J.; Young, A. B.; Abagyan, R.; Feany, M. B.; Hyman, B. T.; Kazantsev, A. G. *Science* **2007**, *317*, 516.
18. Garske, A. L.; Smith, B. C.; Denu, J. M. *ACS Chem. Biol.* **2007**, *2*, 529.
19. Grozinger, C. M.; Chao, E. D.; Blackwell, H. E.; Moazed, D.; Schreiber, S. L. *J. Biol. Chem.* **2001**, *276*, 38837.
20. Tervo, A. J.; Kyrylenko, S.; Niskanen, P.; Salminen, A.; Leppanen, J.; Nyronen, T. H.; Jarvinen, T.; Poso, A. *J. Med. Chem.* **2004**, *47*, 6292.
21. Mai, A.; Massa, S.; Lavu, S.; Pezzi, R.; Simeoni, S.; Ragno, R.; Mariotti, F. R.; Chiani, F.; Camilloni, G.; Sinclair, D. A. *J. Med. Chem.* **2005**, *48*, 7789.
22. Napper, A. D.; Hixon, J.; McDonagh, T.; Keavey, K.; Pons, J. F.; Barker, J.; Yau, W. T.; Amouzegh, P.; Flegg, A.; Hamelin, E.; Thomas, R. J.; Kates, M.; Jones, S.; Navia, M. A.; Saunders, J. O.; DiStefano, P. S.; Curtis, R. *J. Med. Chem.* **2005**, *48*, 8045.
23. Kiviranta, P. H.; Leppanen, J.; Kyrylenko, S.; Salo, H. S.; Lahtela-Kakkonen, M.; Tervo, A.; Wittekindt, C.; Suuronen, T.; Kuusisto, E.; Jarvinen, T.; Salminen, A.; Poso, A.; Wallen, E. A. *J. Med. Chem.* **2006**, *49*, 7907.
24. Heltweg, B.; Gatbonton, T.; Schuler, A. D.; Posakony, J.; Li, H.; Goehle, S.; Kollipara, R.; DePinho, R. A.; Gu, Y.; Simon, J. A.; Bedalov, A. *Cancer Res.* **2006**, *66*, 4368.
25. Trapp, J.; Jochum, A.; Meier, R.; Saunders, L.; Marshall, B.; Kunick, C.; Verdin, E.; Goekjian, P.; Sippl, W.; Jung, M. *J. Med. Chem.* **2006**, *49*, 7307.
26. Trapp, J.; Meier, R.; Hongwiset, D.; Kassack, M. U.; Sippl, W.; Jung, M. *ChemMedChem* **2007**, *2*, 1419.
27. Gey, C.; Kyrylenko, S.; Hennig, L.; Nguyen, L. H.; Buttner, A.; Pham, H. D.; Giannis, A. *Angew. Chem., Int. Ed.* **2007**, *46*, 5219.

28. Tervo, A. J.; Suuronen, T.; Kyrylenko, S.; Kuusisto, E.; Kiviranta, P. H.; Salminen, A.; Leppanen, J.; Poso, A. *J. Med. Chem.* **2006**, *49*, 7239.
29. Kiviranta, P. H.; Leppanen, J.; Rinne, V. M.; Suuronen, T.; Kyrylenko, O.; Kyrylenko, S.; Kuusisto, E.; Tervo, A. J.; Jarvinen, T.; Salminen, A.; Poso, A.; Wallen, E. A. *Bioorg. Med. Chem. Lett.* **2007**, *17*, 2448.
30. Finnin, M. S.; Donigian, J. R.; Pavletich, N. P. *Nat. Struct. Biol.* **2001**, *8*, 621.
31. Huhtiniemi, T.; Wittekindt, C.; Laitinen, T.; Leppanen, J.; Salminen, A.; Poso, A.; Lahtela-Kakkonen, M. *J. Comput. Aided Mol. Des.* **2006**, *20*, 589.
32. Neugebauer, R. C.; Uchiechowska, U.; Meier, R.; Hruby, H.; Valkov, V.; Verdin, E.; Sippl, W.; Jung, M. *J. Med. Chem.* **2008**, *51*, 1203.
33. Garcia-Lopez, M. T.; Gonzalez-Muniz, R.; Molinero, M. T.; Naranjo, J. R.; Del Rio, J. *J. Med. Chem.* **1987**, *30*, 1658.
34. Lin, J. H.; Perryman, A. L.; Schames, J. R.; McCammon, J. A. *J. Am. Chem. Soc.* **2002**, *124*, 5632.
35. Lin, J. H.; Perryman, A. L.; Schames, J. R.; McCammon, J. A. *Biopolymers* **2003**, *68*, 47.
36. Bottegoni, G.; Cavalli, A.; Recanatini, M. *J. Chem. Inf. Model.* **2006**, *46*, 852.
37. Kelley, L. A.; Gardner, S. P.; Sutcliffe, M. J. *Protein Eng.* **1997**, *10*, 737.
38. Avalos, J. L.; Celic, I.; Muhammad, S.; Cosgrove, M. S.; Boeke, J. D.; Wolberger, C. *Mol. Cell* **2002**, *10*, 523.
39. Warren, G. L.; Andrews, C. W.; Capelli, A. M.; Clarke, B.; LaLonde, J.; Lambert, M. H.; Lindvall, M.; Nevins, N.; Semus, S. F.; Senger, S.; Tedesco, G.; Wall, I. D.; Woolven, J. M.; Peishoff, C. E.; Head, M. S. *J. Med. Chem.* **2006**, *49*, 5912.
40. Leach, A. R.; Shoichet, B. K.; Peishoff, C. E. *J. Med. Chem.* **2006**, *49*, 5851.
41. Andrianaivoravelona, J. O.; Terreaux, C.; Sahpaz, S.; Rasolondramanitra, J.; Hostettmann, K. *Phytochemistry* **1999**, *52*, 1145.
42. Sato, H.; Kawgishi, H.; Nishimura, T.; Yoneyama, S.; Yoshimoto, Y.; Sakamura, S.; Furusaki, A.; Katsuragi, S.; Matsumoto, T. *Agric. Biol. Chem.* **1985**, *49*, 2969.
43. Takii, T.; Kawashima, S.; Chiba, T.; Hayashi, H.; Hayashi, M.; Hiroma, H.; Kimura, H.; Inukai, Y.; Shibata, Y.; Nagatsu, A.; Sakakibara, J.; Oomoto, Y.; Hirose, K.; Onozaki, K. *Int. Immunopharmacol.* **2003**, *3*, 273.
44. Van Der Spoel, D.; Lindahl, E.; Hess, B.; Groenhof, G.; Mark, A. E.; Berendsen, H. J. *J. Comput. Chem.* **2005**, *26*, 1701.
45. van Gunsteren, W. F; Billeter, S. R.; Eising, A. A.; Hünenberger, P. H.; Krüger, P.; Mark, A. E.; Scott, W. R. P.; Tironi, I. G. In *Biomolecular Simulation: The GROMOS96 Manual and User Guide*, Hochschulverlag AG an der ETH Zürich: Zürich, Switzerland, 1996.
46. Berendsen, H. J. C.; Postma, J. P. M.; van Gunsteren, W. F.; Hermans, J. In *Intermolecular Forces*; Pullman, B., Ed.; D. Reidel Publishing Company Dordrecht, 1981; pp 331–342.
47. Darden, T.; York, D.; Pedersen, L. *J. Chem. Phys.* **1993**, *98*, 10089.
48. Essmann, U.; Perera, L.; Berkowitz, M. L.; Darden, T.; Lee, H.; Pedersen, L. G. *J. Chem. Phys.* **1995**, *103*, 8577.
49. Berendsen, H. J. C.; Postma, J. P. M.; DiNola, A.; Haak, J. R. *J. Chem. Phys.* **1984**, *81*, 3684.
50. Daura, X.; Gademann, K.; Jaun, B.; Seebach, J. D.; van Gunsteren, W. F.; Mark, A. E. *Angew. Chem., Int. Ed.* **1999**, *38*, 236.
51. Sybyl 7.3, Tripos International, 1699 South Hanley Rd., St. Louis, Missouri, 63144, USA.
52. Jones, G.; Willett, P.; Glen, R. C.; Leach, A. R.; Taylor, R. *J. Mol. Biol.* **1997**, *267*, 727.
53. In R Development Core Team (2005). R: A language and environment for statistical computing. R Foundation for Statistical Computing, Vienna, Austria, 2008. http://www.R-project.org.